

Adipose tissue-derived microvascular fragments promote lymphangiogenesis in a murine lymphedema model

Florian S Frueh¹ , Laura Gassert¹, Claudia Scheuer¹,
Andreas Müller², Peter Fries², Anne S Boewe¹,
Emmanuel Ampofo¹ , Claudia E Rube³, Michael D Menger¹
and Matthias W Laschke¹ 

Abstract

Chronic lymphedema after cancer treatment is common and there is still no cure for this disease. We herein investigated the lymphangiogenic capacity of adipose tissue-derived microvascular fragments (MVF), which contain stem cells and lymphatic vessel fragments. Secondary lymphedema was induced in the hindlimbs of C57BL/6J mice. Green fluorescence protein (GFP)⁺ MVF were isolated from transgenic C57BL/6Tg (CAG-EGFP)1Osb/J mice, suspended in collagen hydrogel, and injected in the lymphadenectomy defect of wild-type animals. This crossover model allowed the detection of MVF-derived blood and lymphatic vessels after transplantation. The MVF group was compared with animals receiving collagen hydrogel only or a sham intervention. Lymphangiogenic effects were analyzed using volumetry, magnetic resonance (MR) lymphography, histology, and immunohistochemistry. MVF injection resulted in reduced hindlimb volumes when compared to non-treated controls. MR lymphography revealed lymphatic regeneration with reduced dermal backflow after MVF treatment. Finally, MVF transplantation promoted popliteal angiogenesis and lymphangiogenesis associated with a significantly increased microvessel and lymphatic vessel density. These findings indicate that MVF transplantation represents a promising approach to induce therapeutic lymphangiogenesis.

Keywords

Lymphangiogenesis, lymphedema, magnetic resonance lymphography, microvascular fragments, tissue engineering

Date received: 5 April 2022; accepted: 12 June 2022

Introduction

Secondary lymphedema is a complex and lifelong disease, which is characterized by damage to the lymphatic vasculature and ultimately leads to impaired immune response, fibrosis, and fatty degeneration of the connective tissue.¹ In developed countries breast cancer treatment is the most common cause for lymphedema, affecting millions of patients.² Consequently, innovative approaches for the therapy of lymphatic vascular insufficiency are investigated by an increasing number of research groups. In the last decades, several treatment strategies have been suggested to tackle lymphedema, including reconstructive microsurgery,^{3,4} pharmacological approaches^{5,6} or lymphatic tissue engineering.⁷ Specifically for the latter,

experimental evidence is scarce because mimicking lymphedema in animal models is challenging.⁸

¹Institute for Clinical and Experimental Surgery, Saarland University, Homburg/Saar, Germany

²Clinic of Diagnostic and Interventional Radiology, Saarland University Medical Center, Homburg/Saar, Germany

³Department of Radiotherapy and Radiation Oncology, Saarland University Medical Centre, Homburg/Saar, Germany

Corresponding author:

Florian S Frueh, Institute for Clinical and Experimental Surgery, Saarland University, Kirrbergerstrasse, Homburg/Saar 66421, Germany.

Email: frueh.flo@gmx.ch



Engineering of the lymphatic vasculature is an emerging field of research aiming at the functional restoration of lymph flow.⁹ This can be achieved by (i) lymphangiogenic cues such as growth factors, (ii) cell-based approaches, (iii) scaffold-based approaches, or (iv) a combination thereof.¹⁰ From the clinician's perspective, engineering strategies based on adipose tissue-derived mesenchymal stem/stromal cells (ADSC) are particularly appealing due to an easily accessible and available source.¹¹ Moreover, ADSC have been shown to induce lymphangiogenesis both *in vitro*¹² as well as *in vivo*.¹³ Recent evidence indicates that ADSC are potent promoters of lymphangiogenesis via direct differentiation into lymphatic endothelial cells (LEC) and via paracrine stimulation.¹³ In clinical pilot studies, the injection of adipose tissue-derived regenerative cells for the treatment of breast cancer-related lymphedema has already been taken from bench to bedside.^{14,15}

Adipose tissue-derived microvascular fragments (MVF) represent powerful angiogenic units that have been used to enhance the vascularization of skin substitutes.^{16–20} In contrast to single cells, the isolation protocol for MVF is characterized by a shorter enzymatic adipose digestion, retaining a physiological microvessel morphology.²¹ Hence, the formation of microvascular networks within MVF-seeded scaffolds is much faster than within single cell-seeded implants, because MVF only have to reconnect to each other and inosculate with the surrounding host microvasculature.²² Importantly, MVF also stimulate the regeneration of lymphatic vessels, as previously found in MVF-enriched skin substitutes^{16,17} and porous polyethylene scaffolds.²³ In line with this, the visceral adipose tissue of mice contains a recently described lymphatic vascular network.^{24,25} Therefore, MVF may not only contain ADSC but also lymphatic vessel fragments and it can be assumed that they are particularly suitable building blocks for lymphatic tissue engineering.^{16,26} In the present study, this hypothesis was tested by investigating the lymphangiogenic effects of MVF in a murine hindlimb lymphedema model. For that purpose, lymphedema was induced using irradiation and popliteal lymphadenectomy. MVF suspended in collagen hydrogel were injected in the lymphadenectomy defect. The MVF group was compared with animals receiving collagen hydrogel only or a sham intervention, respectively. Lymphangiogenic effects were analyzed by means of volumetry, magnetic resonance (MR) lymphography, histology, and immunohistochemistry.

Material and methods

Animals

For the induction of lymphedema, male C57BL/6J mice (Institute for Clinical and Experimental Surgery, Saarland University, Homburg/Saar, Germany) with a body weight of >24 g were used. MVF were harvested from male C57BL/6-Tg(CAG-EGFP)10sb/J mice (The Jackson Laboratory, Bar Harbor, ME, USA) with a body weight of

≥30 g. All animals were housed one per cage with a 12-h day/night cycle while being fed *ad libitum* with water and standard pellet food (Atromin, Lage, Germany).

Isolation of MVF

MVF were obtained as previously described.^{16,21} Briefly, the bilateral epididymal fat pads of male C57BL/6-Tg(CAG-EGFP)10sb/J mice were harvested, transferred into 10% Dulbecco's modified eagle medium (DMEM; 10% fetal calf serum (FCS), 100 U/mL penicillin, 0.1 mg/mL streptomycin; Biochrom GmbH, Berlin, Germany) and washed thrice with phosphate-buffered saline (PBS; Biochrom GmbH). Thereafter, the fat was minced and digested for ~10 min with collagenase NB4G (0.5 U/mL; Serva Electrophoresis GmbH, Heidelberg, Germany) while stirring under humidified atmospheric conditions. The digestion was stopped by neutralization with 20% FCS in PBS. The resulting cell-vessel suspension was incubated twice for 5 min at 37°C for cell-vessel sedimentation and fat supernatant was eliminated. The remaining largely fat-free cell-vessel suspension was filtered through a 500 µm mesh (pluriSelect Life Science, Leipzig, Germany) and centrifuged for 5 min at 600 × g.

Flow cytometric analysis of MVF

To evaluate the fraction of lymphatic endothelial cells contained in MVF, we performed flow cytometric analyses. For this purpose, MVF from eight donor mice were pooled into four separate isolates and digested in Accutase (BioLegend, Fell, Germany) for 15 min into single cells. Subsequently, the cells were analyzed for the expression of the endothelial cell marker CD31 with the monoclonal rat anti-mouse CD31-PE antibody (BD Pharmingen, Heidelberg, Germany). Moreover, the expression of the lymphatic endothelial cell markers prospero homeobox (Prox)1 and lymphatic vessel endothelial hyaluronan receptor (LYVE)-1 was analyzed with the monoclonal rabbit anti-mouse Prox1-FITC (Biorbyt, Cambridge, UK) and the monoclonal rat anti-mouse LYVE-1-PE (R&D Systems) antibodies. Isotype-identical rat IgG2κ-PE (BD Pharmingen) and rabbit IgG-FITC (Biorbyt) antibodies served as IgG controls. All flow cytometric analyses were performed by means of a FACScan (BD Biosciences). Data were assessed using the software package Cell-Quest Pro (BD Biosciences).

Quantitative real-time polymerase chain reaction (qRT-PCR). To analyze the expression of angiogenic and lymphangiogenic genes in isolated MVF, pooled MVF from three donor mice were cultivated in DMEM under hypoxia (95% N₂, 5% CO₂, and 1% O₂) or normoxia for 6 h. Thereafter, the total RNA was extracted with QIAzol lysis reagent and transcribed into cDNA by using qScriber (highQu, Kraichtal, Germany) according to the manufacturer's protocol. qRT-PCR analysis was performed by using ORA™ SEE qPCR Green ROX L

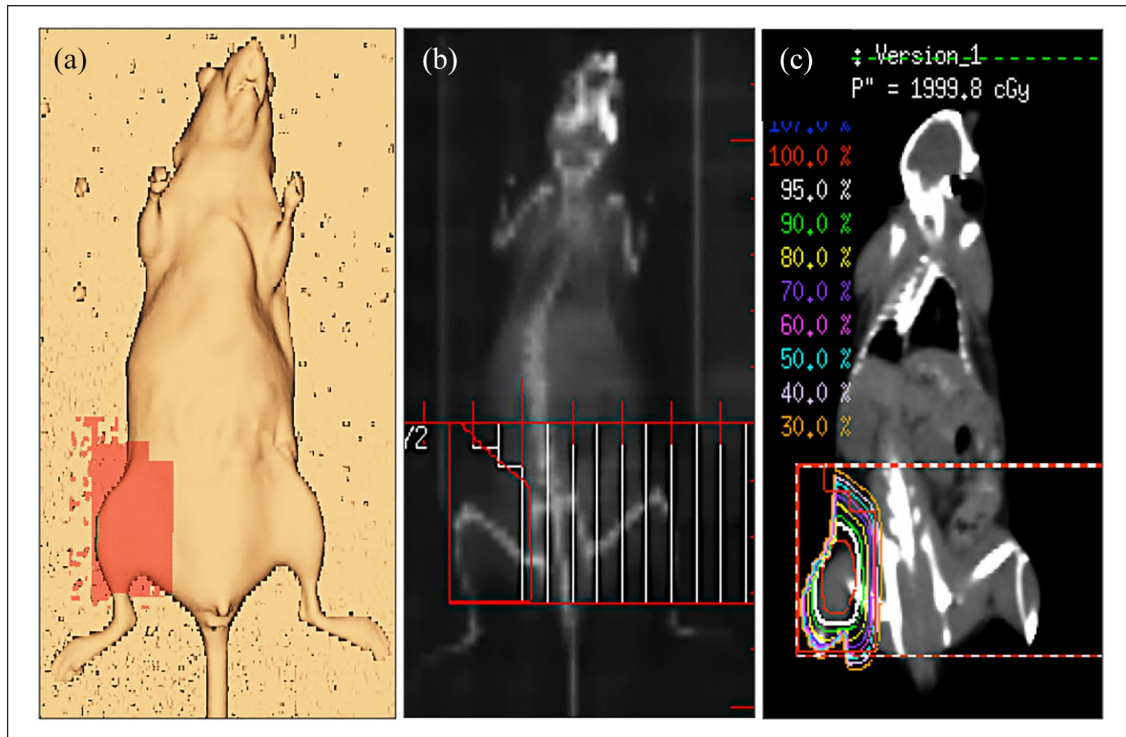


Figure 1. Radiotherapy. (a) Radiotherapy planning in the right groin of a C57BL/6J mouse, (b) digitally reconstructed radiograph with multileaf collimator field used for irradiation, and (c) coronal computed tomography image with isodose lines illustrating the dose distribution.

Mix (highQu, Kraichtal, Germany). The following forward and reverse primers were used at a concentration of 100 nM: Vascular endothelial growth factor (VEGF)-A forward 5'-GACAGAAGGAGAGCAGAAGT-3' and reverse 5'-TCTCAATCGGACGGCAGTA-3'; VEGF-C forward 5'-CTGATGTCTGTCCTGTACCC-3' and reverse 5'-TCCCCACATCTATACACACC-3'; VEGF-D forward 5'-GATCCGAGCAGCTTCTAGTT-3' and reverse 5'-GTGAGTCCATACTGGCAAGA-3'; insulin-like growth factor (IGF)-1 forward 5'-GATGCTCTTCAGTTCGTGTG-3' and reverse 5'-CACAGCTCCGGAAGCAACAC-3'; LYVE-1 forward 5'-CTCA AACACCCGCAACAG-3' and reverse 5'-TTCGTTCTTGAATGCTGCTC-3'; Prox1 forward 5'-CACCAGGGATTGTGAGCTAT-3' and reverse 5'-AACTCCCCTAACGTGATCTG-3'; glyceraldehyde-3-phosphate dehydrogenase (GAPDH) forward 5'-CGGTGCTGAGTATGTC-3' and reverse 5'-TTTGGCTCCACCCTTC-3'. GAPDH was used as endogenous control. Data collection was performed by means of a CFX96™ real-time system (Bio-Rad Laboratories, Feldkirchen, Germany) and the $2^{-\Delta\Delta Ct}$ method.

Animal model

Lymphedema was induced in the right hindlimb of C57BL/6J mice by a combined lymphatic ablation using irradiation and subsequent popliteal lymphadenectomy.

For irradiation planning, a representative mouse was scanned with a computed tomography scanner (Brilliance

Big Bore CT; Philips Healthcare, Eindhoven, The Netherlands). This planning data set was used to define the planning target volume (PTV) in the right groin of the animals and the treatment plan was calculated using the Pinnacle v9.8 (Philips Healthcare) planning system (Figure 1(a)–(c)). The PTV was irradiated with a single dose of 20 Gy using a 6 MV photon multi leaf collimator field from anterior direction. The animals were anesthetized by intraperitoneal injection of ketamine (75 mg/kg body weight; Ursotamin, Serumwerke Bernburg AG, Bernburg, Germany) and xylazine (15 mg/kg body weight; Rompun, Bayer, Leverkusen, Germany).

Ten days after irradiation, a popliteal lymphadenectomy was performed as previously reported.²⁷ For this purpose, hindlimbs were depilated and after intradermal injection of methylene blue 10% (Carl Roth GmbH, Karlsruhe, Germany) in the paw, a circular skin incision was performed over the popliteal fossa. The afferent lymphatic vessels were ligated with 10/0 monofilament (Monosof; Covidien Deutschland GmbH, Neustadt/Donau, Germany) and the popliteal lymph node including the perinodal fat pad and the efferent lymphatic vessels were resected under microscopic magnification. The skin was closed with interrupted 5/0 monofilament (Prolene; Ethicon, Johnson & Johnson Medical GmbH, Norderstedt, Germany). Postoperative analgesia was provided for 3 days with tramalhydrochloride (40 mg/100 mL drinking water; Grünenthal GmbH, Aachen, Germany). The

non-operated contralateral hindlimbs served as internal control.

Preparation of MVF-enriched collagen hydrogel

MVF were harvested from five male C57BL/6-Tg(CAG-EGFP)10sb/J donor mice. This transgenic mouse line is transfected with enhanced green fluorescent protein (GFP) cDNA under the control of a chicken β -actin promoter and cytomegalovirus enhancer. Accordingly, all tissues of these mice except red blood cells and hair appear green under blue light excitation.²⁸ After transplantation into GFP⁻ wild-type mice, this approach allows an easy detection of MVF-derived blood and lymphatic vessels by their GFP⁺ signal.^{16,29} A total of 5 mL adipose tissue was used for the preparation of MVF-enriched hydrogel. After isolation, the GFP⁺ MVF pellet was mixed with 200 μ L of a collagen hydrogel (400 μ L collagen 0.4% [Serva Electrophoresis GmbH], 50 μ L 10 \times RPMI 1640, 2.45 μ L Hepes 1 M and 1.75 μ L NaOH 0.7 M [Sigma-Aldrich Chemie GmbH, Taufkirchen, Germany]).

Hydrogel injection into lymphadenectomy defect site

Three days after lymphadenectomy, the animals of the collagen and collagen/MVF groups were anesthetized and single popliteal sutures were released. Using a precision pipette, a volume of 20 μ L of the collagen hydrogel was then applied with a precision pipette into the popliteal tissue defect of each animal of the collagen group. The animals of the collagen/MVF group were injected with a volume of 20 μ L MVF-enriched collagen hydrogel, equivalent to the MVF amount of 500 μ L fat pad volume or approximately 20,000 individual MVF.³⁰ Animals of the control group underwent a sham procedure without injection, that is, suture release with wound irrigation and skin closure.

Hindlimb volumetry

Repetitive assessment of hindlimb volumes was performed every other day throughout the course of the *in vivo* experiment. The animals were anesthetized with 1.5% isoflurane and an electronic caliper was used to evaluate the paw thickness, which represents an established surrogate parameter for rodent hindlimb volumes.^{27,31} In addition, partial hindlimb volumes were calculated based on axial MR images by modifying a previously described technique.²⁷

MR imaging (MRI)

Mice were examined in a horizontal-bore 9.4 T animal scanner (BioSpec Avance III 94/20; Bruker Biospin GmbH, Ettlingen, Germany) equipped with a BGA12S gradient system (maximum field strength, 675 mT m⁻¹;

linear inductive rise time, 130 μ s; maximum slew rate, 4673 mT m⁻¹ s⁻¹). ParaVision 6.0.1 (Bruker Biospin GmbH) served as operating software. The animals were placed in supine position and transferred to the magnet tail-first. Imaging was performed using a linearly polarized coil developed for imaging of the entire mouse body with an inner diameter of 40 mm (Bruker Biospin GmbH). We acquired a coronal 3-dimensional (3D) gradient recalled echo (GRE) time-of-flight (TOF) sequence adjusted to the blood flow velocity with a high spatial resolution resulting in a voxel size of 75 μ m³. MRI measurements were performed with 4 averages before and directly after injection of the experimental contrast agent. Scan duration was 8 min 46 s. MRI sequence parameter details are provided in supplementary data (Supplemental Table 1).

Contrast agent

For interstitial MR lymphography, the nanoparticle AGuIX was used. This contrast agent has a rather small molecular mass of 8.5 \pm 1.0 kDa with a mean hydrodynamic diameter of 3.0 \pm 1.0 nm. It has been established as a contrast agent for interstitial MR lymphography in rats.³¹ For injection, AGuIX was freshly prepared at a concentration of 3 mM AGuIX, 145 mM NaCl, 2 mM CaCl₂·6 H₂O, 5 mM HEPES, pH 7.4 from a sterile filtrated stock solution and sterile pure water (Aqua ad iniectabilia, B. Braun Melsungen AG, Melsungen, Germany). For MR lymphography, the fourth phalanx of both hindlimbs was injected intradermally with 10 μ L of the contrast medium preparations using a precision syringe with 31-gage needles (Hamilton Bonaduz AG, Bonaduz, Switzerland).

Processing of MRI data

Imaging datasets were transferred in DICOM format to an external workstation. For MR lymphography demonstrating lymphatic regeneration, maximum intensity projections (MIP) were generated with OsiriX v.4.1.2 software (Pixmeo Sarl, Bernex, Switzerland) and saved in coronal orientation.

For partial hindlimb volumetry as well as for signal-to-noise-ratio (SNR) measurements after contrast medium injection, multiplanar reconstructions on the original 3D datasets were performed in axial orientation using OsiriX. Resolution was kept identical to the initially recorded 3D datasets. Axial images were saved as separate DICOM series, anonymized and exported by investigator I (AM). Images were then transferred to investigator II (PF) for blinded partial volume measurements and SNR recordings.

Partial MR volumetry

Partial MR volumetry was performed on an axial multiplanar reconstruction series. For standardization, these slices

were centered around the distal tibio-fibular joint, that is, the center slice plus four slices above and below the joint.²⁷ In these images, regions of interest (ROIs) were drawn precisely enclosing the hindlimbs. To calculate the partial volumes, areas covered by the individual ROI were recorded in mm², transferred to an Excel file, multiplied by slice thickness (0.75 μ m) and added together.²⁷

SNR measurements for dermal backflow quantification

As a semi-quantitative surrogate parameter for dermal backflow, SNR was quantified in the entire dermis of individual axial slices from the data sets reconstructed for partial volumetry. ROIs were created covering the entire dermis. Signal intensities (SI) in these ROIs were recorded and used to calculate SNR as follows

$$\text{SNR} = \text{SI}_{\text{dermal ROI}} / \text{noise}$$

Noise was measured as average standard deviation (SD) of the background signal collected from one circular ROI sized identically for all images investigated. These ROIs were placed in identical positions in the air ventral to the animals and between their legs.

Histology and immunohistochemistry

Formalin-fixed tissue samples were embedded in paraffin and cut into 3–4 μ m-thick sections. Individual sections were stained with hematoxylin and eosin (HE) according to standard procedures. Using a BX60 microscope (Olympus, Hamburg, Germany) and the imaging software cellSens Dimension 1.11 (Olympus), the epidermal thickness (given in μ m) of the paws was quantified in the center of every other high-power field (HPF, area = 0.09 mm²) of each sample at 400 \times magnification. To quantify adipose tissue accumulation, further sections were stained with perilipin. The number of perilipin⁺ fat vacuoles was evaluated in randomly selected HPFs of each sample.

For the immunohistochemical detection of myeloperoxidase (MPO)⁺ neutrophilic granulocytes, sections were incubated with a rabbit polyclonal anti-MPO antibody (1:100; Abcam, Cambridge, UK) as primary antibody. This was followed by a biotinylated goat anti-rabbit IgG antibody (ready-to-use; Abcam). The biotinylated antibody was detected by peroxidase-labeled streptavidin (ready-to-use; Abcam). 3-Amino-9-ethylcarbazole (Abcam) was used as chromogen and the sections were counterstained with Mayer's hemalum (Merck, Darmstadt, Germany). Finally, the number of MPO⁺ cells was evaluated in at least five randomly selected HPFs per section using the BX60 microscope.

For the immunohistochemical analysis of subcutaneous blood and lymphatic vessels, additional sections were

stained with a monoclonal rat anti-mouse antibody against CD31 (1:100; dianova GmbH, Hamburg, Germany) and a polyclonal rabbit antibody against lymphatic vessel endothelial hyaluronan receptor-1 (LYVE-1; 1:200; Abcam). A goat anti-rat IgG-Alexa555 antibody (1:100; Molecular Probes, Eugene, OR, USA) and a goat anti-rabbit IgG-Alexa555 antibody (1:200; Molecular Probes) served as secondary antibodies. Cell nuclei were stained with Hoechst 33342 (2 μ g/mL; Sigma-Aldrich Chemie GmbH). To quantify the lymphatic vessel area (given in % of total area), at least three randomized HPFs per section were analyzed. Blood and lymphatic vessel density (given in mm⁻²) were evaluated in different histological zones. Zone I represented the area directly underneath the popliteal incision while zones II and III represented more peripheral scar tissue. The density of blood and lymphatic vessels of the central zone was evaluated based on 1 HPF per sample and that of the peripheral zones based on 2 HPFs per sample, respectively.

Finally, the fraction of CD31⁺/GFP⁺ blood and LYVE-1⁺/GFP⁺ lymphatic vessels (given in %) was assessed. To differentiate between MVF-derived GFP⁺ and wild-type GFP⁻ blood and lymphatic vessels, sections were stained with the above-mentioned primary and secondary antibodies against CD31 and LYVE-1 and with a polyclonal goat anti-GFP antibody (1:100; Rockland, Limerick, PA). A biotin-labeled donkey anti-goat IgG antibody (1:100; Molecular Probes) was used as secondary antibody and detected by fluorescein labeled-streptavidin (1:50; Molecular Probes). For this purpose, sections were placed in Coplin jars with 0.05% citraconic anhydride solution (pH 7.4) for 1 h at 98°C and incubated overnight at 4°C with the primary antibody, followed by the secondary antibody at 37°C for 2 h.

Experimental protocol

In a first set of in vitro experiments, the cellular composition and gene expression of MVF was investigated (11 donor animals). For the subsequent in vivo experiments, three groups were used ($n=10$ animals/group): (i) control group, (ii) collagen group, and (iii) collagen/MVF group. Irradiation was performed on day (d)-10 with popliteal lymphadenectomy on d0 (Figure 2(a)). On d3, MVF were isolated from five transgenic animals for the fabrication of MVF-enriched collagen hydrogel. The control group underwent a sham procedure and the collagen and collagen/MVF groups received popliteal injection of collagen and collagen/MVF, respectively (Figure 2(a)). On d14 and d28 after lymphadenectomy, MR lymphography was performed and the animals were sacrificed on d28 for histological and immunohistochemical analyses (Figure 2(a)). Due to infection at the surgical site, two animals in the control group and one animal in the collagen as well as in the collagen/MVF group were excluded from the study.

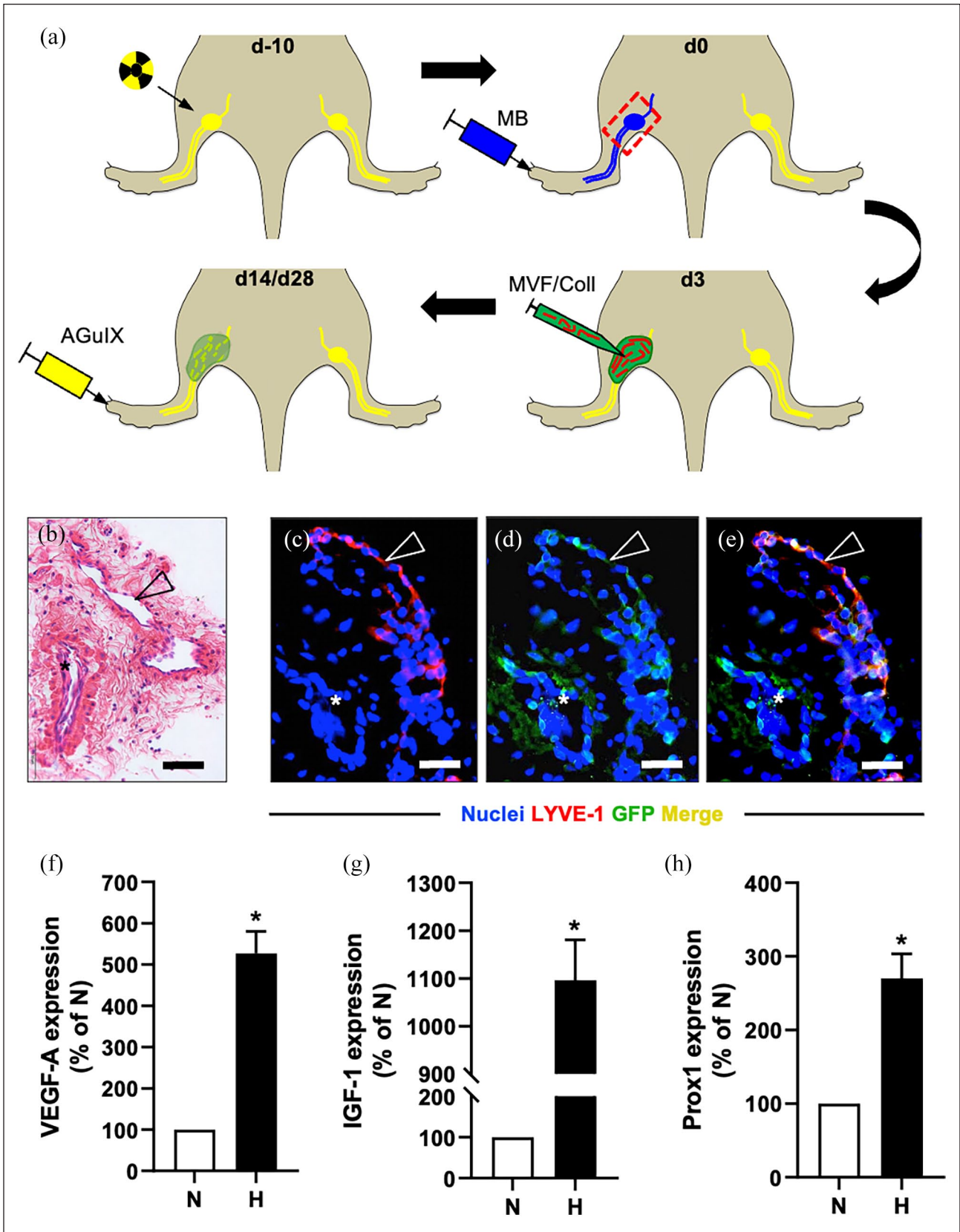


Figure 2. (Continued)

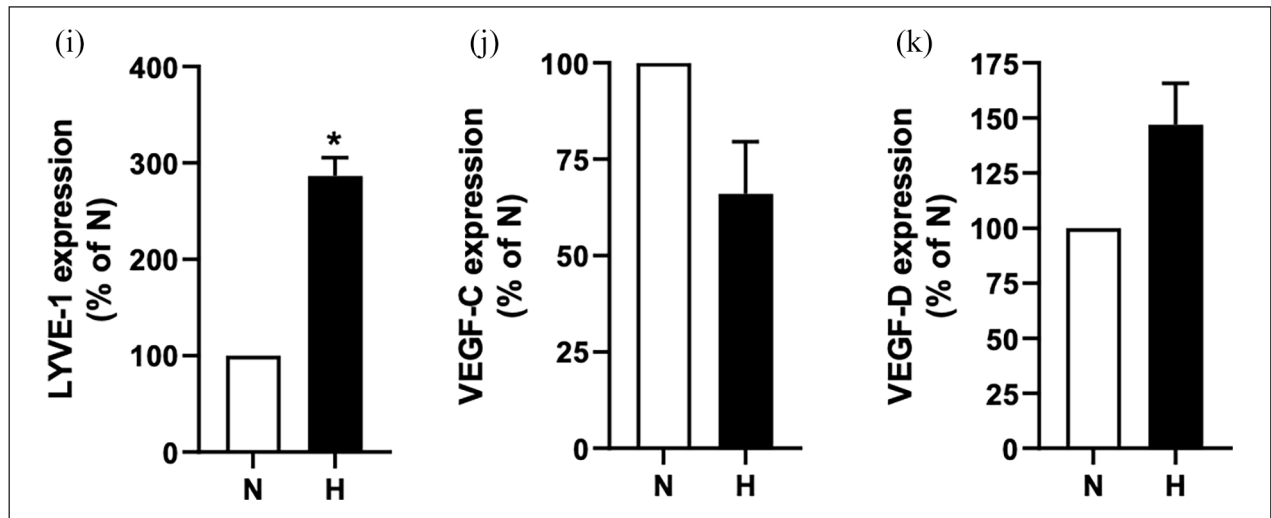


Figure 2. Study design and MVF characterization. Study design (a): Combined lymphatic ablation by means of irradiation (top left) and popliteal lymphadenectomy 10 days later (top right, red frame = lymphadenectomy site). For identification of the popliteal lymphatic system, hindlimbs were injected with methylene blue. Three days after lymphadenectomy, MVF (red)-enriched collagen hydrogel (green) was injected in the popliteal defect (bottom right). On day 14 and 28, repetitive MR lymphography using the nanoparticle AgulX was performed to evaluate lymphatic regeneration (bottom left). HE-stained (b) and immunohistochemical (c–e) sections of in vitro suspended collagen/MVF hydrogel, revealing LYVE-1⁺/GFP⁺ lymphatic (arrowhead) and LYVE-1⁻/GFP⁺ blood vessel fragments (asterisk). Scale bars: (b) = 50 μ m, (c–e) = 30 μ m. Quantitative analysis of mRNA expression levels in normoxic (N) and hypoxic (H) MVF (f–k). VEGF-A (f), IGF-1 (g), Prox1 (h), LYVE-1 (i), VEGF-C (j), and VEGF-D (k) mRNA levels are expressed in % normoxia ($n=3$). Mean \pm SEM. * $p < 0.05$ versus normoxia. Coll: collagen; GFP: green fluorescent protein; HE: hematoxylin and eosin; IGF: insulin-like growth factor; LYVE: lymphatic vessel endothelial hyaluronan receptor; MB: methylene blue; MR: magnetic resonance; MVF: microvascular fragments; VEGF: vascular endothelial growth factor.

Statistics

Data were analyzed for normal distribution and equal variance. Two groups were compared using the paired *t*-test (parametric data) or the Wilcoxon signed rank test (non-parametric data). Multiple groups with normal distribution were compared using one-way analysis of variance followed by the Dunnett's post hoc test. In case of non-parametric distribution, groups were analyzed with the Kruskal-Wallis test followed by the Dunn's post hoc test. Data are given as mean \pm standard error of the mean (SEM). Statistical significance was accepted for $p < 0.05$. The statistical analysis was performed using Prism 9 (GraphPad Software, Inc.).

Results

Cellular composition and gene expression of MVF

The cellular composition of isolated MVF was evaluated by means of flow cytometry. The MVF contained $42 \pm 2\%$ cells positive for the pan-endothelial cell marker CD31. Further analyses showed that $22 \pm 3\%$, and $13 \pm 2\%$ cells expressed the lymphatic endothelial cell markers Prox1 and LYVE-1, respectively. Double staining confirmed these findings with $21 \pm 2\%$ Prox1⁺/CD31⁺ cells and

$12 \pm 1\%$ LYVE-1⁺/CD31⁺ cells. In line with this finding, histological and immunohistochemical stainings of the collagen/MVF suspension revealed lymphatic vessel fragments characterized by a LYVE-1⁺/GFP⁺ endothelium (Figure 2(b)–(e)).

In addition, the expression of different angiogenic and lymphangiogenic genes in isolated MVF was analyzed under normoxia and hypoxia by means of qRT-PCR (Figure 2(f)–(k)). The expression of VEGF-A, IGF-1, Prox1, and LYVE-1 was significantly upregulated in hypoxic MVF when compared to normoxic controls (Figure 2(f)–(i)). In contrast, the expression of VEGF-D was only slightly increased, whereas VEGF-C was downregulated (Figure 2(j) and (k)).

Animal model validation

Combined lymphatic ablation resulted in a significant and persistent swelling of the operated hindlimbs throughout the 28-days course of the experiment compared to the healthy contralateral side (Figure 3(a)–(c)). Further investigations revealed that the subcutaneous tissue of the operated hindlimbs exhibited histological hallmarks of persistent lymphedema on day 28. In fact, we found a markedly larger area of LYVE-1⁺ lymphatic vessels, indicating lymphatic stasis (Figure 3(d)–(f)).

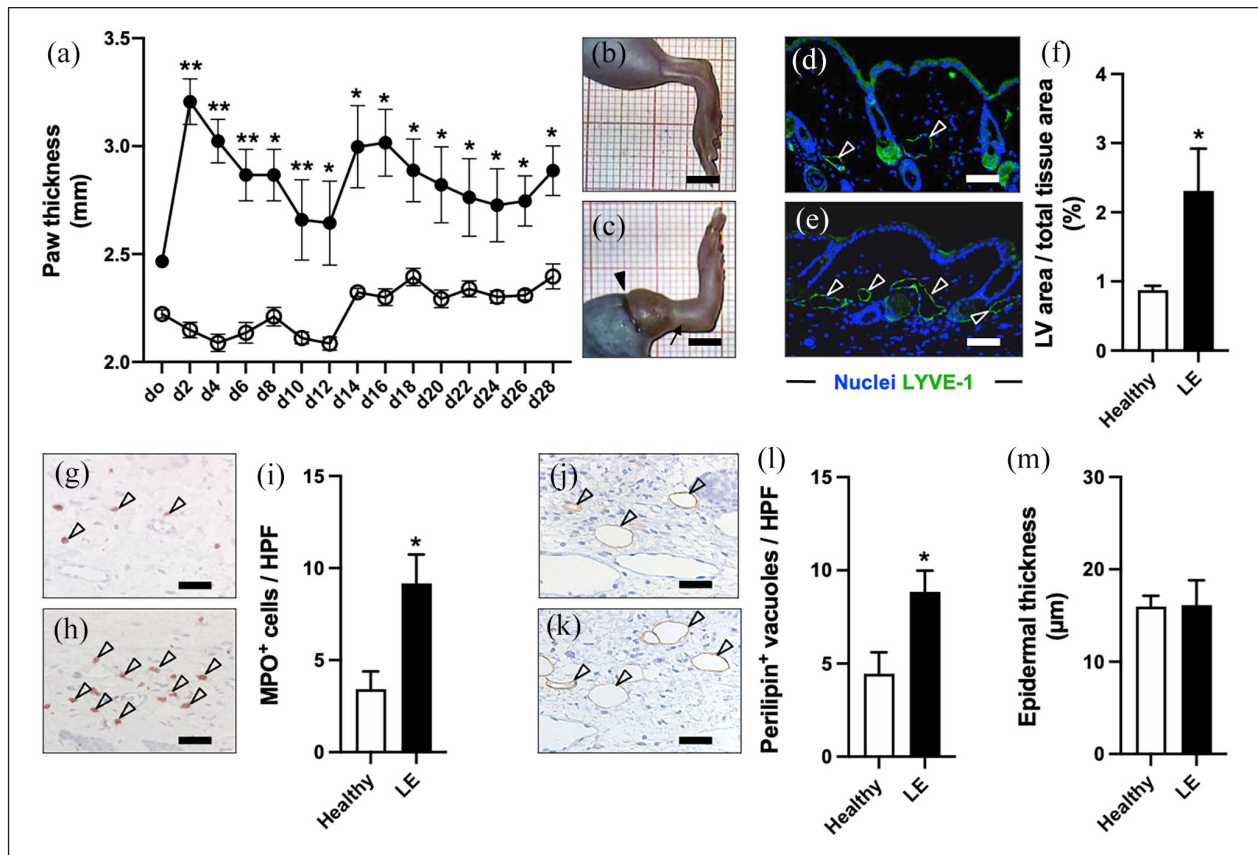


Figure 3. Animal model validation. LE evaluation over 28 days by means of paw thickness measurements ((a) black dots = LE, white dots = healthy). Representative stereomicroscopic images of healthy (b) and LE (c) hindlimbs on day 28 with persistent swelling (arrow in (c)) of the operated limb (arrowhead = lymphadenectomy scar). LYVE-1⁺ dermal lymphatic vessels (arrowheads) on day 28 in healthy (d) and LE (e) hindlimbs. Quantification of lymphatic vessel area per total tissue area in % (f). Infiltration of MPO⁺ neutrophilic granulocytes (arrowheads) in healthy (g) and LE (h) hindlimbs. Quantification of MPO⁺ cells per HPF (i). Perilipin⁺ fat vacuoles (arrowheads) in healthy (j) and LE (k) hindlimbs. Quantification of perilipin⁺ vacuoles per HPF (l). Quantification of epidermal thickness in µm (m). (a, f, i, l, and m) Mean ± SEM, $n=8$, * $p < 0.05$ versus healthy, ** $p < 0.001$ versus healthy. Scale bars: (b) and (c) = 5 mm, (d, e, g, h, j, and k) = 60 µm. HPF: high-power field; LE: lymphedema; LV: lymphatic vessel; LYVE: lymphatic vessel endothelial hyaluronan receptor; MPO: myeloperoxidase.

Moreover, increased inflammatory cell infiltration as well as adipose deposition was observed in the operated hindlimbs (Figure 3(g)–(l)). In contrast, the epidermal thickness of lymphedema and healthy hindlimbs was not significantly different (Figure 3(m)).

Lymphatic network formation and dermal backflow after MVF transplantation

In subsequent analyses, the regeneration of the lymphatic system was investigated in the control, collagen and collagen/MVF groups. Qualitative MR lymphography was performed 14 and 28 days after lymphadenectomy to visualize lymphatic network formation (Figure 4). This imaging technique allowed for a high-resolution visualization of the lymphatic system, as indicated in MR scans of healthy hindlimbs. The two collecting lymphatic vessels

could be identified draining to the popliteal lymph node (Figure 4(a)). In lymphedema hindlimbs of the control group, focal dermal backflow was observed on day 14 and 28 with minimal formation of lymphatic collaterals (Figure 4(a)). In contrast, popliteal injection of collagen and collagen/MVF stimulated lymphatic network formation (Figure 4(b) and (c)). Additionally, in the collagen/MVF group, collateral lymphatic drainage to the inguinal lymph node was observed (Figure 4(c)).

In a subset of experiments, dermal backflow was quantified on axial MR lymphography images (Figure 5). We found that the amount of epifascial contrast agent in non-treated lymphedema hindlimbs of the control group remained constantly elevated 14 as well as 28 days after lymphadenectomy (Figure 5(a)–(d)). In contrast, collagen and collagen/MVF injection was associated with a significantly reduced dermal backflow at both timepoints (Figure 5(d)).

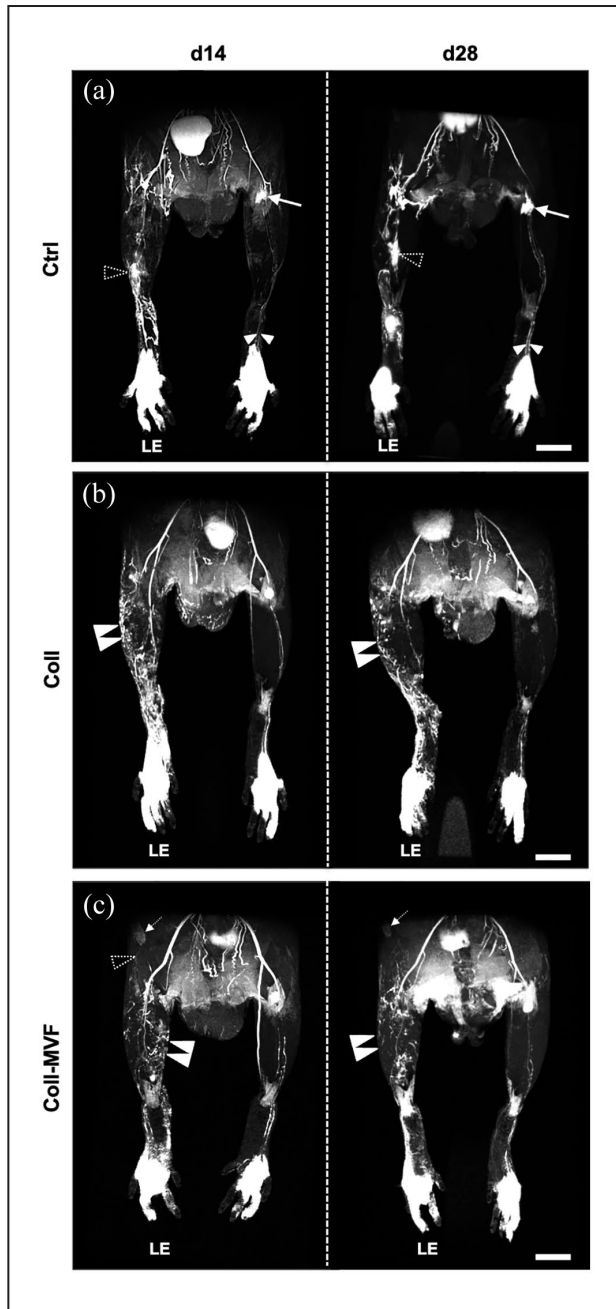


Figure 4. Interstitial MR lymphography after MVF transplantation. 3D coronal hindlimb scans of the control (a), collagen (b) and collagen/MVF (c) group. The paired collecting lymphatic vessels ((a) white arrowheads) draining to the popliteal lymph node ((a) arrow) are well detectable in healthy hindlimbs. In contrast, LE hindlimbs exhibit persistent dermal backflow ((a), dashed arrowheads) and only minor lymphatic regeneration. After collagen and collagen/MVF injection, a collateral lymphatic network ((b and c) double arrowheads) with reduced dermal backflow is observed on day 14 and 28. Lymphatic drainage ((c) dashed arrowhead) to the inguinal lymph node ((c), dashed arrow) in the collagen/MVF group. Scale bars: (a–c) = 5 mm. Coll: collagen; Ctrl: control; LE: lymphedema; MR: magnetic resonance; MVF: microvascular fragments.

Hindlimb volume, lymphatic vessel area, inflammatory cell infiltration, adipose deposition, and dermal thickness after MVF transplantation

Hindlimb volumetry was performed by repetitive assessment of partial limb volumes and paw thickness. No relevant difference among the groups was found for the partial hindlimb volumes on day 14 or 28 (Figure 5(e)). However, the mean paw thickness of the collagen and collagen/MVF groups was significantly lower at the end of the 28-days experiment when compared to non-treated controls (Figure 5(f)). Of note, collagen or collagen/MVF injection did not result in a significant reduction of lymphatic vessel area, inflammatory cell infiltration, adipose deposition or dermal thickness of hindlimb paws compared to the control group (data not shown).

Popliteal microvessel density after MVF transplantation

Histological analyses of the hindlimbs at the level of the lymphadenectomy were performed at the end of the experiment to evaluate the effect of collagen and collagen/MVF application on tissue vascularization (Figure 6). The microvascular density was quantified in three histological zones with a centripetal orientation from the popliteal scar (Figure 6(a)–(c)). In the collagen/MVF group, the scar tissue contained a rich plexus of GFP⁺ blood and lymphatic vessels (Figure 6(d)). Immunohistochemical detection of CD31⁺ microvessels revealed a significantly increased overall microvessel density in the collagen/MVF group when compared to the collagen and non-treated group (Figure 6(e)–(h)). Furthermore, collagen/MVF injection resulted in a significantly higher angiogenic activity with markedly more CD31⁺ microvessels even in the peripheral zones II/III (Figure 6(i)). Finally, CD31/GFP co-staining showed that 98 ± 1% of the analyzed microvessels were GFP⁺, indicating their origin from the transplanted MVF.

Popliteal lymphatic vessel density after MVF transplantation

To evaluate the effect of MVF transplantation on the popliteal lymphatic vasculature, immunohistochemical detection of LYVE-1⁺ lymphatic vessels was performed (Figure 7(a)–(c)). Importantly, the overall lymphatic vessel density was significantly increased in the collagen/MVF group when compared to the collagen and non-treated control group (Figure 7(d)). Moreover, the percentage of GFP⁺ and therefore MVF-derived lymphatic vessels was high (85 ± 5%). Subzone analyses revealed a trend toward an elevated lymphatic vessel density in the central zone I, which, however, was not proven to be significant (Figure 7(e)).

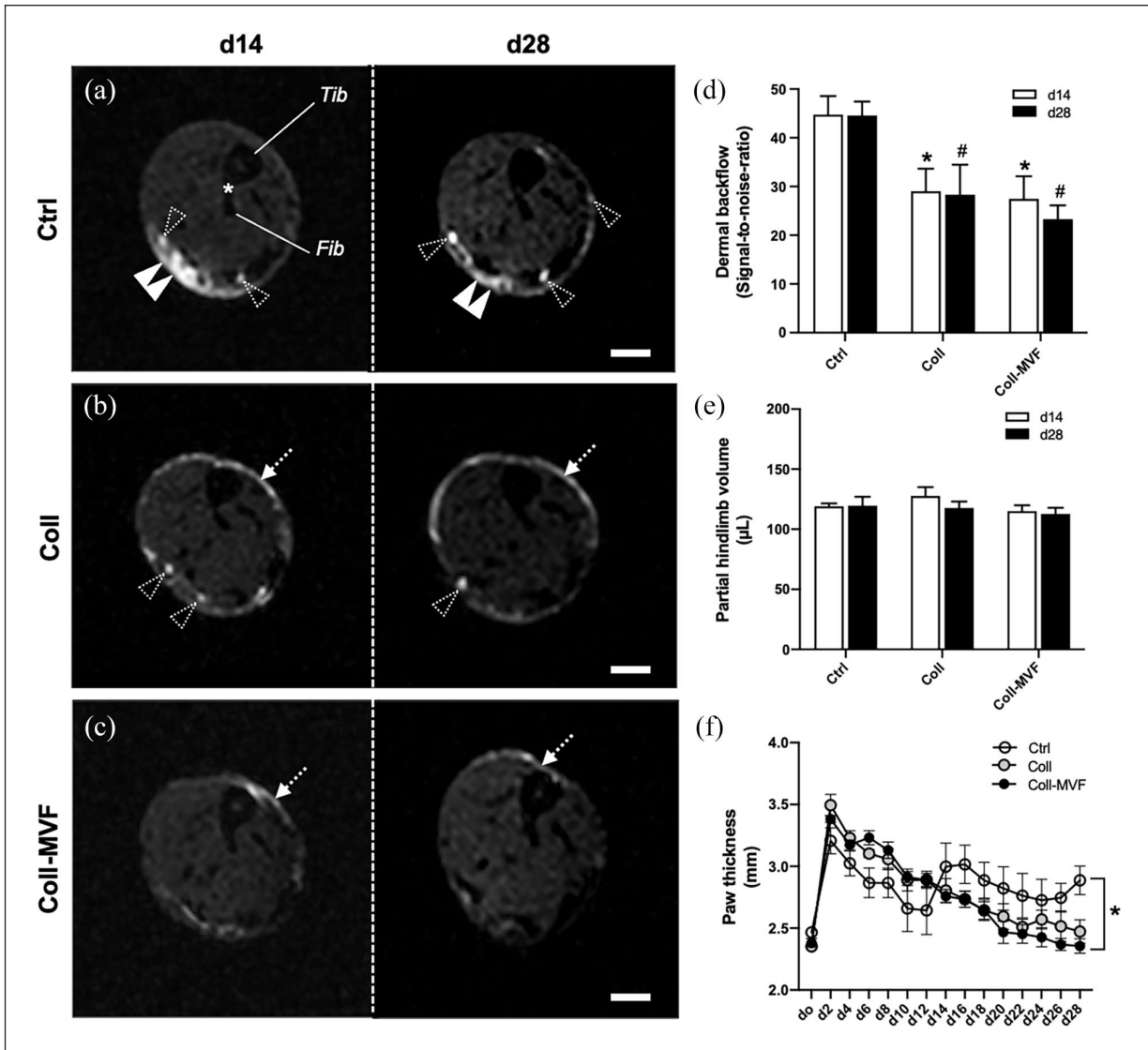


Figure 5. Volumetry and dermal backflow after MVF transplantation. Axial MR lymphography scans of control (a), collagen (b), and collagen/MVF (c) LE hindlimbs at the level of the distal tibio-fibular joint (asterisk) 14 and 28 days after lymphadenectomy. Dermal backflow ((a) double arrowheads) is observed in all groups with a significant reduction in the collagen and collagen/MVF groups ((b and c) dashed arrows). Dashed arrowheads: individual lymphatic vessels, Fib: fibula; Tib: tibia. Quantification of dermal backflow (d). * $p < 0.05$ versus Ctrl day 14, # $p < 0.05$ versus Ctrl day 28. Mean \pm SEM, $n = 8$. Quantification of hindlimb volumes by means of MR volumetry (e) and paw thickness measurements (f). * $p < 0.05$ versus Ctrl. Mean \pm SEM, $n = 8-9$. Scale bars = 1 mm. Coll: collagen; Ctrl: control; LE: lymphedema; MR: magnetic resonance; MVF: microvascular fragments.

Discussion

Tissue engineering of the blood vascular system has made major progress in the last years. In contrast, engineering of the lymphatic system is still in its infancy. This is remarkable since the importance of lymphangiogenesis for many biological processes is well described.^{1,32,33} Moreover, lymphangiogenesis may also be critical for the integration of bioengineered scaffolds.^{7,16,34} A clinically relevant target for lymphatic tissue engineering is the restoration of lymphatic function in lymphedema. Currently, there is no cure for this lifelong and debilitating disease and successful

engineering of the lymphatic system might pave the way for novel therapeutic approaches. Therefore, we herein investigated whether adipose tissue-derived MVF are able to tackle secondary lymphedema in mice.

Beside abundant microvessels, the visceral adipose tissue of mice also contains a dense network of lymphatic vessels.^{24,25} Consequently, MVF isolated from epididymal fat pads should be rich of lymphatic vessel fragments.²⁶ Indeed, we found that MVF contained individual LYVE-1⁺ lymphatic vessel fragments adjacent to the microvasculature. This novel finding was supported by flow cytometric

analyses of MVF, revealing that up to 22% of their cellular components stained positive for the lymphatic endothelial cell marker Prox1. This indicates a surprisingly high fraction of lymphatic endothelial cells within MVF.

However, the lymphatic vasculature may be more fragile to mechanical and enzymatic degradation when compared to microvessels. Hence, future experiments are necessary to evaluate the functional integrity of lymphatic vessel

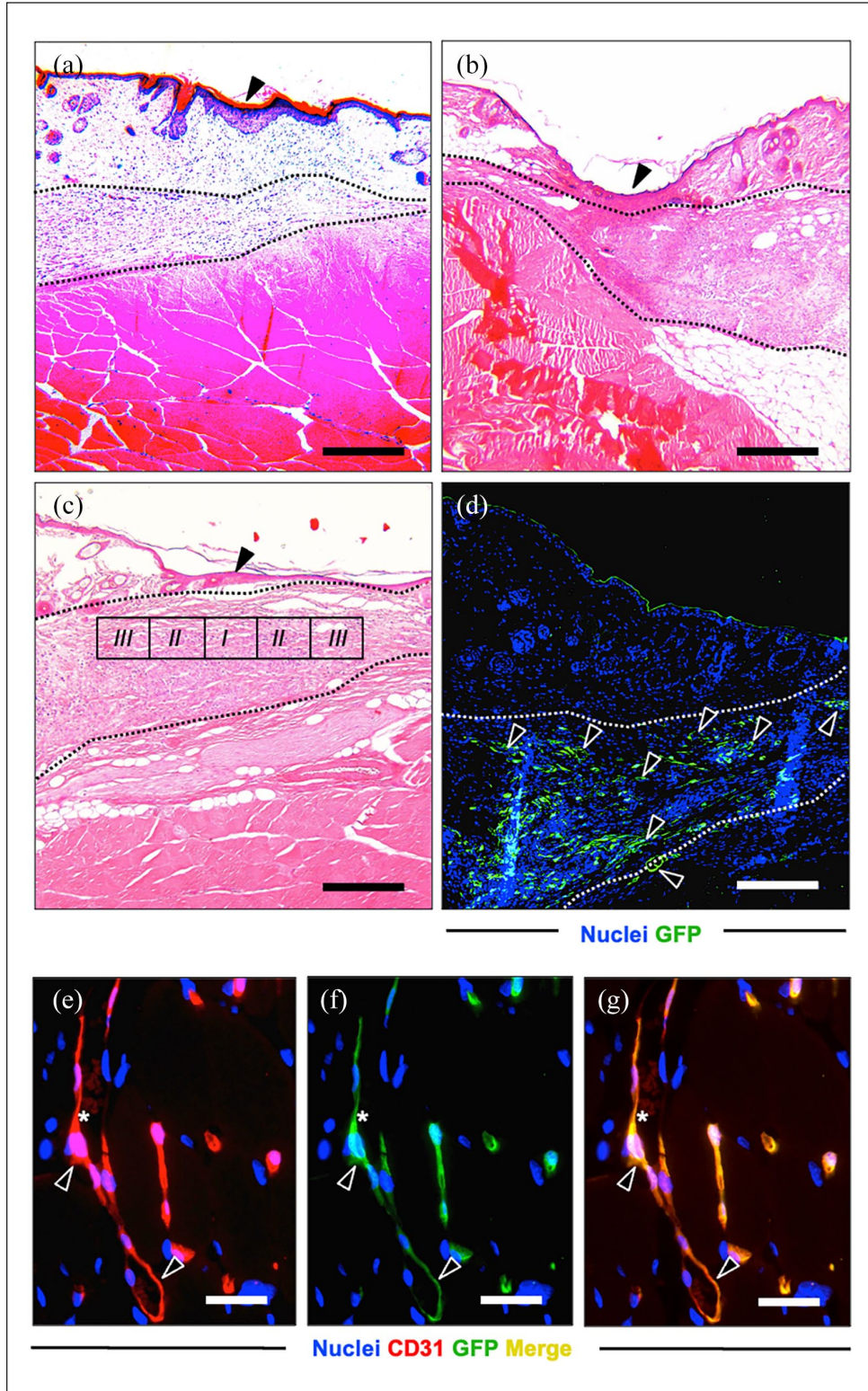


Figure 6. (Continued)

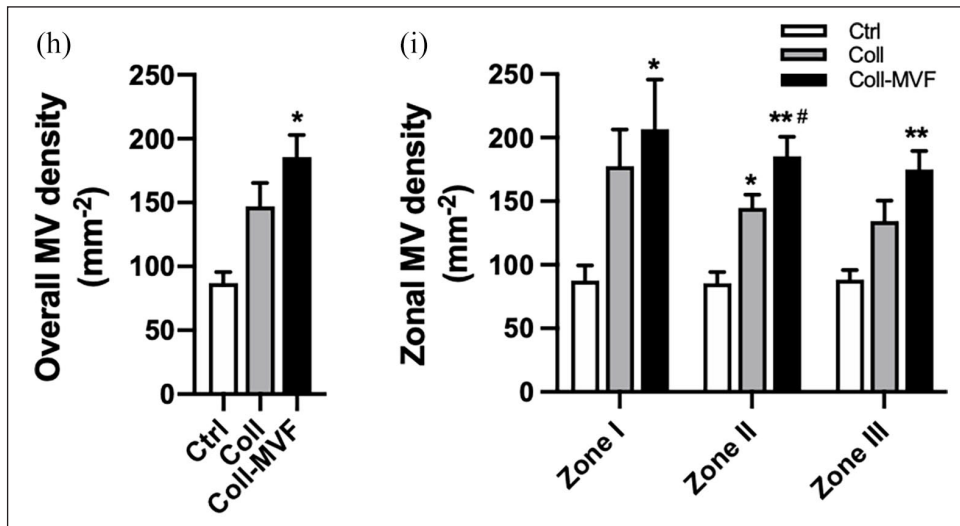


Figure 6. Popliteal microvessel density after MVF transplantation. HE-stained (a–c) and GFP-stained (d) sections of the popliteal fossa of the control (a), collagen (b) and collagen/MVF (c and d) groups 28 days after lymphadenectomy. Arrowheads in (a–c) = lymphadenectomy scar. Area between dashed lines = epifascial collagen (b) and collagen/MVF (c and d) deposits. Popliteal GFP⁺ MVF-derived blood and lymphatic vessels ((d), arrowheads). Immunohistochemical detection (e–g) of a MVF-derived CD31⁺/GFP⁺ microvessel (arrowheads) filled with erythrocytes (asterisks). Quantification of overall MV density in mm⁻² (h). Quantification of zonal MV density in mm⁻² (i). Mean \pm SEM, $n = 8–9$, * $p < 0.05$ versus Ctrl, ** $p < 0.001$ versus Ctrl, # $p < 0.05$ versus Coll. Scale bars: (a–d) = 200 μ m, (e–g) = 30 μ m. Coll: collagen; Ctrl = control; GFP: green fluorescent protein; MV: microvessel; MVF: microvascular fragments.

fragments after MVF isolation. Recent investigations revealed that the visceral adipose tissue of humans contains lymphatic capillaries and larger lymphatic vessels.³⁵ In contrast, the subcutaneous fat is characterized by scarce lymphatic vascular structures and no initial lymphatics were found.³⁵ From a translational perspective this finding is important since subcutaneous adipose tissue may not be the ideal source to obtain regenerative cells and lymphatic vessel fragments for therapeutic lymphangiogenesis.

The induction of secondary lymphedema in the mouse hindlimb mimicking the chronic nature of human disease is difficult due to the high regenerative capacity of the rodent lymphatic system.^{8,36} In previous rat hindlimb experiments we found that the combination of irradiation and lymphadenectomy results in lymphatic dysfunction characterized by histopathological hallmarks of secondary lymphedema, such as tissue fibrosis, immune cell infiltration, and an increase in lymphatic vessel area.³¹ In contrast to more invasive hindlimb rodent models,³⁷ circular skin incisions were closed directly and not sutured down to the muscle.³¹ In the current study, mice underwent a similar procedure with direct closure of the popliteal incision. This detail is crucial, because it allows to inject MVF into the lymphatic defect with repetitive evaluation by means of volumetry and MR lymphography. However, direct skin closure is commonly associated with moderate lymphedema and less pronounced volumetric and histopathological changes when compared to more invasive models,³⁷ rendering the evaluation of therapeutic

interventions even more challenging. In the control group, the combined lymphatic ablation resulted in increased hindlimb volumes throughout the 28-day course of the experiment compared to non-operated hindlimbs. Furthermore, we found an increased lymphatic vessel area, inflammatory cell infiltration as well as adipose deposition in control hindlimbs, validating our animal model with sustained secondary lymphedema.

Experimental MR imaging of the lymphatic vasculature in rodents is rarely used due to small animal size, high technological costs and non-specific distribution of commercially available contrast agents.^{38,39} We previously validated the nanoparticle AGuIX for interstitial MR lymphography in rats.³¹ In the present study, AGuIX-based MR lymphography at 9.4T yielded high-resolution insights into lymphatic network formation of the mouse hindlimb. Remarkably, persistent dermal backflow and scarce lymphatic collaterals were found in the control group when compared to the animals of the collagen and collagen/MVF groups. These findings indicate that collagen as well as collagen/MVF injection are able to stimulate lymphangiogenesis. Consequently, collagen hydrogel alone may also exert significant lymphangiogenic effects. In line with this, nanofibrillar collagen scaffolds have recently been shown to enhance lymphatic regeneration in preclinical⁴⁰ and clinical⁴¹ studies. In our investigation, however, the lymphangiogenic findings observed in MR lymphography of the collagen group could not be supported by immunohistochemistry.

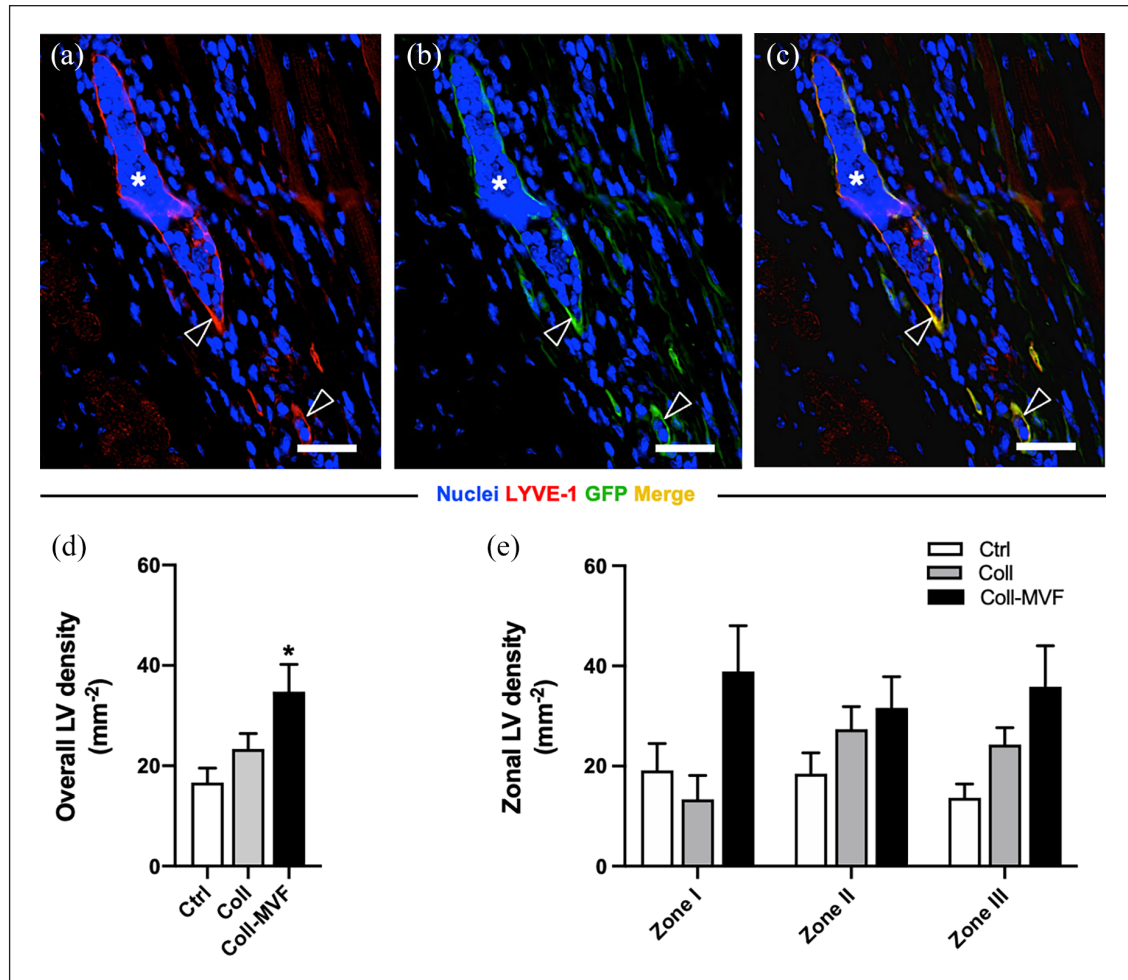


Figure 7. Popliteal lymphatic vessel density after MVF transplantation. Immunohistochemical detection (a–c) of MVF-derived LYVE-1⁺/GFP⁺ lymphatic vessels (arrowheads). Scale bars = 30 μm. Quantification of overall LV density in mm⁻² (d). Quantification of zonal LV density in mm⁻² (e). Mean ± SEM, n = 8–9, *p < 0.05 versus Ctrl. Coll: collagen; Ctrl: control; GFP: green fluorescent protein; LV: lymphatic vessel; LYVE: lymphatic vessel endothelial hyaluronan receptor; MVF: microvascular fragments.

To evaluate lymphatic function after collagen/MVF injection, additional volumetric and histopathological analyses were performed. Hindlimb volumetry by means of repetitive paw thickness measurements revealed that collagen/MVF injection resulted in a markedly reduced swelling on day 28 when compared to controls. However, the volume reduction was not associated with improved histopathological hallmarks of secondary lymphedema. Hence, the lymphatic collaterals identified on MR imaging may not have been sufficient to significantly reduce lymphatic stasis in the herein used animal model. Further limitations of this study include a relatively short observation period and the lack of dynamic and functional lymphatic imaging, such as near-infrared imaging⁴² or lymphoscintigraphy.⁴³ The incorporation of these imaging technologies could have been helpful to better understand the functional relevance of MVF-derived lymphatic regeneration.

In recent skin tissue engineering experiments, MVF-seeded skin substitutes were characterized by a strong

stimulation of blood and lymphatic vessel network formation.^{16,17} Subsequent investigations on MVF-coated scaffolds for craniofacial reconstruction confirmed a promising MVF-derived lymphangiogenesis.²³ In the current study, we evaluated popliteal blood and lymphatic vessel densities after MVF injection in the lymphadenectomy wound. Immunohistochemical analyses revealed that the injection of collagen/MVF but not collagen alone resulted in a significantly higher microvessel density when compared to non-treated controls. Furthermore, nearly all analyzed microvessels were CD31⁺/GFP⁺, hence originated from the transplanted MVF. Finally, MVF-derived vascularization was observed in all zones of the popliteal scar. These results confirm a strong angiogenic effect of MVF. Our findings are in line with the results of Pilia et al.⁴⁴ who reported high tissue perfusion after collagen/MVF transplantation in a mouse hindlimb model of volumetric muscle loss. Of note, they also found a significantly higher angiogenic potential of MVF compared with ADSC transplantation.

To investigate the impact of MVF transplantation on popliteal lymphangiogenesis, LYVE-1/GFP co-staining was performed. Interestingly, we found an overall higher lymphatic vessel density after collagen/MVF injection compared with samples of the control and collagen groups. However, in contrast to blood vessel formation, the lymphangiogenic effect was less pronounced and a smaller yet relevant fraction of the lymphatic vessels stained positive for LYVE-1/GFP, which is similar to other investigations on MVF-promoted lymphangiogenesis.^{16,17} To mimic the ischemic conditions during the initial post-transplant phase *in vitro*, we additionally analyzed the effect of hypoxia on the expression of angiogenic and lymphangiogenic genes in isolated MVF. In line with the results of Flann *et al.*⁴⁵ we detected an upregulated gene expression of VEGF-A and IGF-1, which is most probably caused by hypoxia-inducible factor (HIF)-1 α . We additionally investigated the expression of VEGF-C and VEGF-D, which are major regulators involved in lymphangiogenesis.⁴⁶ However, the expression of the two proteins did not significantly differ between normoxia and hypoxia. This can be explained by the fact that the VEGF-C and the VEGF-D promoter do not contain a hypoxia response element and therefore do not respond to HIF-1 α -mediated gene transcription. Prox1 and LYVE-1 are not only marker proteins of lymphatic endothelial cells but are also involved in cell proliferation and migration.^{47,48} Zhou *et al.* demonstrated that hypoxia increases the expression of Prox1.⁴⁹ Moreover, Prox1 acts as a positive regulator of LYVE-1 gene expression.⁵⁰ Accordingly, we herein found an upregulation of both proteins under hypoxia. These results indicate that the higher number of blood and lymphatic vessels in the collagen/MVF group of our *vivo* experiments may have been driven by different hypoxia-induced signaling pathways within the grafted MVF.

This is the first study evaluating MVF transplantation for lymphedema treatment. In future studies, this approach should be compared to ADSC-based engineering of the lymphatic system. Of note, preclinical work on ADSC for lymphatic tissue engineering has been performed in different experimental models of lymphedema, such as the mouse tail or hindlimb.⁵¹ While paracrine stimulation of lymphangiogenesis was a consistent finding after ADSC application,^{13,52–57} ADSC differentiation into lymphatic endothelial cells was less commonly observed.^{13,56} Beside blood and lymphatic vessel fragments, MVF also contain a relevant fraction of ADSC.¹⁸ Therefore, they may not only induce lymphangiogenesis through lymphatic vessel fragment or lymphatic endothelial cell transfer but also through stem cell-mediated paracrine effects. However, it still remains elusive whether lymphatic vessel fragments are indeed able to reconnect to a functional network or whether in the present study lymphangiogenesis was predominantly driven by paracrine stimulation and differentiation.

Nonetheless, the possible interplay of lymphatic vessel fragments and single cell-mediated lymphangiogenesis makes MVF highly interesting for lymphatic tissue engineering.

Conclusion

MVF transplantation is a novel experimental approach to induce therapeutic lymphangiogenesis. Since MVF contain regenerative adipose tissue-derived single cells as well as lymphatic vessel fragments, they are particularly promising for lymphatic tissue engineering. In a hindlimb model of secondary lymphedema, MVF stimulated the formation of lymphatic collaterals, leading to a reduction of dermal back-flow. MVF transplantation was also associated with an increased popliteal blood and lymphatic vessel density and, ultimately, reduction of hindlimb volumes.

Acknowledgements

We are grateful for the excellent assistance of Janine Becker, Caroline Bickelmann, Stephanie Kremp, Norbert Licht, Ruth Nickels, and Julia Parakenings.

Declaration of conflicting interests

The author(s) declared no potential conflicts of interest with respect to the research, authorship, and/or publication of this article.

Funding


The author(s) disclosed receipt of the following financial support for the research, authorship, and/or publication of this article: Florian S. Frueh received support from the German Society for Lymphology (DGL, grant number Fo0315) and S&T AG Microsurgical Instruments, Neuhausen, Switzerland.

Ethical approval

The local governmental animal protection committee (Landesamt für Verbraucherschutz, Saarbrücken, Germany) approved all experiments (permit number: 48/2015). They were conducted in accordance with the European legislation on the protection of animals (Directive 2010/63/EU) and the NIH guidelines on the care and use of laboratory animals (NIH publication #85-23 Rev. 1985).

ORCID iDs

Florian S Frueh  <https://orcid.org/0000-0003-0904-9591>

Emmanuel Ampofo  <https://orcid.org/0000-0002-1886-5657>

Matthias W Laschke  <https://orcid.org/0000-0002-7847-8456>

Supplemental material

Supplemental material for this article is available online.

Availability of data and materials

Data not available in the manuscript can be obtained from the corresponding author on reasonable request.

References

- Alitalo K, Tammela T and Petrova TV. Lymphangiogenesis in development and human disease. *Nature* 2005; 438: 946–953.
- Dayan JH, Ly CL, Kataru RP, et al. Lymphedema: Pathogenesis and novel therapies. *Annu Rev Med* 2018; 69: 263–276.
- Beederman M, Garza RM, Agarwal S, et al. Outcomes for physiologic microsurgical treatment of secondary lymphedema involving the extremity. *Ann Surg* 2020; DOI: 10.1097/SLA.0000000000004457.
- Hong JPJ, Song S and Suh HSP. Supermicrosurgery: principles and applications. *J Surg Oncol* 2018; 118: 832–839.
- Mehrara BJ, Park HJ, Kataru RP, et al. Pilot study of anti-Th2 immunotherapy for the treatment of breast cancer-related upper extremity lymphedema. *Biology* 2021; 10: 934.
- Gardenier JC, Kataru RP, Hespe GE, et al. Topical tacrolimus for the treatment of secondary lymphedema. *Nat Commun* 2017; 8: 14345.
- Spörlein A, Will PA, Kilian K, et al. Lymphatic tissue engineering: a further step for successful lymphedema treatment. *J Reconstr Microsurg* 2021; 37: 465–474.
- Frueh FS, Gousopoulos E, Rezaeian F, et al. Animal models in surgical lymphedema research – a systematic review. *J Surg Res* 2016; 200: 208–220.
- Alderfer L, Wei A and Hanjaya-Putra D. Lymphatic tissue engineering and regeneration. *J Biol Eng* 2018; 12: 32.
- Asaad M and Hanson SE. Tissue engineering strategies for cancer-related lymphedema. *Tissue Eng Part A* 2021; 27: 489–499.
- Chen K, Sinelnikov MY, Reshetov IV, et al. Therapeutic potential of mesenchymal stem cells for postmastectomy lymphedema: a literature review. *Clin Transl Sci* 2021; 14: 54–61.
- Ahmadzadeh N, Robering JW, Kengelbach-Weigand A, et al. Human adipose-derived stem cells support lymphangiogenesis in vitro by secretion of lymphangiogenic factors. *Exp Cell Res* 2020; 388: 111816.
- Dai T, Jiang Z, Cui C, et al. The roles of Podoplanin-positive/podoplanin-negative cells from adipose-derived stem cells in lymphatic regeneration. *Plast Reconstr Surg* 2020; 145: 420–431.
- Toyserkani NM, Jensen CH, Andersen DC, et al. Treatment of breast cancer-related lymphedema with adipose-derived regenerative cells and fat grafts: a feasibility and safety study. *Stem Cells Transl Med* 2017; 6: 1666–1672.
- Toyserkani NM, Jensen CH, Tabatabaeifar S, et al. Adipose-derived regenerative cells and fat grafting for treating breast cancer-related lymphedema: lymphoscintigraphic evaluation with 1 year of follow-up. *J Plast Reconstr Aesthet Surg* 2019; 72: 71–77.
- Frueh FS, Später T, Lindenblatt N, et al. Adipose tissue-derived microvascular fragments improve vascularization, lymphangiogenesis, and integration of dermal skin substitutes. *J Invest Dermatol* 2017; 137: 217–227.
- Frueh FS, Später T, Körbel C, et al. Prevascularization of dermal substitutes with adipose tissue-derived microvascular fragments enhances early skin grafting. *Sci Rep* 2018; 8: 10977.
- Laschke MW and Menger MD. Adipose tissue-derived microvascular fragments: natural vascularization units for regenerative medicine. *Trends Biotechnol* 2015; 33: 442–448.
- Später T, Menger MM, Nickels RM, et al. Macrophages promote network formation and maturation of transplanted adipose tissue-derived microvascular fragments. *J Tissue Eng* 2020; 11: 2041731420911816.
- Später T, Worringer DM, Menger MM, et al. Systemic low-dose erythropoietin administration improves the vascularization of collagen-glycosaminoglycan matrices seeded with adipose tissue-derived microvascular fragments. *J Tissue Eng* 2021; 12: 20417314211000304.
- Frueh FS, Später T, Scheuer C, et al. Isolation of murine adipose tissue-derived microvascular fragments as vascularization units for tissue engineering. *J Vis Exp* 2017; (122): 55721.
- Später T, Frueh FS, Nickels RM, et al. Prevascularization of collagen-glycosaminoglycan scaffolds: stromal vascular fraction versus adipose tissue-derived microvascular fragments. *J Biol Eng* 2018; 12: 24.
- Später T, Tobias AL, Menger MM, et al. Biological coating with platelet-rich plasma and adipose tissue-derived microvascular fragments improves the vascularization, biocompatibility and tissue incorporation of porous polyethylene. *Acta Biomater* 2020; 108: 194–206.
- Escobedo N and Oliver G. The lymphatic vasculature: its role in adipose metabolism and obesity. *Cell Metab* 2017; 26: 598–609.
- Lackman MH, Subashi Y and Karaman S. A closer look at adipose tissue lymphatics and their markers. *Curr Opin Hematol* 2022; 29: 144–150.
- Laschke MW, Später T and Menger MD. Microvascular fragments: more than just natural vascularization units. *Trends Biotechnol* 2021; 39: 24–33.
- Frueh FS, Körbel C, Gassert L, et al. High-resolution 3D volumetry versus conventional measuring techniques for the assessment of experimental lymphedema in the mouse hindlimb. *Sci Rep* 2016; 6: 34673.
- Okabe M, Ikawa M, Kominami K, et al. ‘Green mice’ as a source of ubiquitous green cells. *FEBS Lett* 1997; 407: 313–319.
- Laschke MW, Kleer S, Scheuer C, et al. Vascularisation of porous scaffolds is improved by incorporation of adipose tissue-derived microvascular fragments. *Eur Cell Mater* 2012; 24: 266–277.
- Später T, Körbel C, Frueh FS, et al. Seeding density is a crucial determinant for the in vivo vascularisation capacity of adipose tissue-derived microvascular fragments. *Eur Cell Mater* 2017; 34: 55–69.
- Müller A, Fries P, Jelvani B, et al. Magnetic resonance lymphography at 9.4 T using a gadolinium-based nanoparticle in rats: Investigations in healthy animals and in a hindlimb lymphedema model. *Invest Radiol* 2017; 52: 725–733.
- Aspelund A, Robciuc MR, Karaman S, et al. Lymphatic system in cardiovascular medicine. *Circ Res* 2016; 118: 515–530.
- Alitalo K. The lymphatic vasculature in disease. *Nat Med* 2011; 17: 1371–1380.
- Schaupper M, Jeltsch M, Rohringer S, et al. Lymphatic vessels in regenerative medicine and tissue engineering. *Tissue Eng Part B Rev* 2016; 22: 395–407.

35. Redondo PAG, Gubert F, Zaverucha-do-Valle C, et al. Lymphatic vessels in human adipose tissue. *Cell Tissue Res* 2020; 379: 511–520.
36. Suzuki Y, Nakajima Y, Nakatani T, et al. Comparison of normal hindlimb lymphatic systems in rats with detours present after lymphatic flow blockage. *PLoS One* 2021; 16: e0260404.
37. Ogino R, Hayashida K, Yamakawa S, et al. Adipose-derived stem cells promote intussusceptive lymphangiogenesis by restricting dermal fibrosis in irradiated tissue of mice. *Int J Mol Sci* 2020; 21: 3885.
38. Kiryu S, Inoue Y, Sheng F, et al. Interstitial MR lymphography in mice: comparative study with gadofluorine 8, gadofluorine M, and gadofluorine P. *Magn Reson Med Sci* 2012; 11: 99–107.
39. Polomska AK and Proulx ST. Imaging technology of the lymphatic system. *Adv Drug Deliv Rev* 2021; 170: 294–311.
40. Hadamitzky C, Zaitseva TS, Bazalova-Carter M, et al. Aligned nanofibrillar collagen scaffolds - guiding lymphangiogenesis for treatment of acquired lymphedema. *Biomaterials* 2016; 102: 259–267.
41. Nguyen DH, Zhou A, Posternak V, et al. Nanofibrillar collagen scaffold enhances edema reduction and formation of new lymphatic collectors after lymphedema surgery. *Plast Reconstr Surg* 2021; 148: 1382–1393.
42. Blum KS, Proulx ST, Luciani P, et al. Dynamics of lymphatic regeneration and flow patterns after lymph node dissection. *Breast Cancer Res Treat* 2013; 139: 81–86.
43. Yang CY, Nguyen DH, Wu CW, et al. Developing a lower limb lymphedema animal model with combined lymphadenectomy and low-dose radiation. *Plast Reconstr Surg Glob Open* 2014; 2: e121.
44. Pilia M, McDaniel J, Guda T, et al. Transplantation and perfusion of microvascular fragments in a rodent model of volumetric muscle loss injury. *Eur Cell Mater* 2014; 28: 11–24; discussion 23–14.
45. Flann KL, Rathbone CR, Cole LC, et al. Hypoxia simultaneously alters satellite cell-mediated angiogenesis and hepatocyte growth factor expression. *J Cell Physiol* 2014; 229: 572–579.
46. Morfoisse F, Renaud E, Hantelys F, et al. Role of hypoxia and vascular endothelial growth factors in lymphangiogenesis. *Mol Cell Oncol* 2014; 1: e29907.
47. Bui K and Hong YK. Ras pathways on Prox1 and lymphangiogenesis: insights for therapeutics. *Front Cardiovasc Med* 2020; 7: 597374.
48. Wu M, Du Y, Liu Y, et al. Low molecular weight hyaluronan induces lymphangiogenesis through LYVE-1-mediated signaling pathways. *PLoS One* 2014; 9: e92857.
49. Zhou B, Si W, Su Z, et al. Transcriptional activation of the prox1 gene by HIF-1 α and HIF-2 α in response to hypoxia. *FEBS Lett* 2013; 587: 724–731.
50. Derynck R and Akhurst RJ. BMP-9 balances endothelial cell fate. *Proc Natl Acad Sci U S A* 2013; 110: 18746–18747.
51. Forte AJ, Boczar D, Sarabia-Estrada R, et al. Use of adipose-derived stem cells in lymphatic tissue engineering and regeneration. *Arch Plast Surg* 2021; 48: 559–567.
52. Yan A, Avraham T, Zampell JC, et al. Adipose-derived stem cells promote lymphangiogenesis in response to VEGF-C stimulation or TGF- β 1 inhibition. *Future Oncol* 2011; 7: 1457–1473.
53. Hayashida K, Yoshida S, Yoshimoto H, et al. Adipose-derived stem cells and vascularized lymph node transfers successfully treat mouse hindlimb secondary lymphedema by early reconnection of the lymphatic system and lymphangiogenesis. *Plast Reconstr Surg* 2017; 139: 639–651.
54. Yoshida S, Hamuy R, Hamada Y, et al. Adipose-derived stem cell transplantation for therapeutic lymphangiogenesis in a mouse secondary lymphedema model. *Regen Med* 2015; 10: 549–562.
55. Ackermann M, Wettstein R, Senaldi C, et al. Impact of platelet rich plasma and adipose stem cells on lymphangiogenesis in a murine tail lymphedema model. *Microvasc Res* 2015; 102: 78–85.
56. Hwang JH, Kim IG, Lee JY, et al. Therapeutic lymphangiogenesis using stem cell and VEGF-C hydrogel. *Biomaterials* 2011; 32: 4415–4423.
57. Shimizu Y, Shibata R, Shintani S, et al. Therapeutic lymphangiogenesis with implantation of adipose-derived regenerative cells. *J Am Heart Assoc* 2012; 1: e000877.